Chapter 9
Design of Rotating Disks and Stress Concentrations

9.1 Failure Criteria

With the usual assumptions of a plane stress state ($\sigma_z = 0$) made for rotating disks, the stress field is generally biaxial. Uniaxial stress conditions can only occur locally: at the inner edge of non-rotating disks loaded at the outer edge (Figs. 2.1 and 2.2) and of only rotating disks (Fig. 2.6), and at the outer edge of non-rotating disks loaded at the inner edge (Figs. 2.3 and 2.4), of rotating annular disks (Fig. 2.6) and rotating solid disks (Fig. 2.15). Biaxial tensile, tensile-compressive and tensile or compressive stress occur respectively at the centre of only rotating disks (Fig. 2.15), at the inner edge of non-rotating annular disks loaded at the inner edge (Figs. 2.3 and 2.4) and at the outer edge of non-rotating annular disks loaded at the outer edge (Figs. 2.1 and 2.2). Biaxial tensile, compressive or tensile-compressive stress conditions occur in the intermediate sections of the disk.

From this overview of stress conditions, we can conclude that strength evaluation of rotating disks calls for the use of a failure criterion. In this area, the criteria in current use are the maximum normal stress criterion (σ_{max}), the maximum strain criterion (ε_{max}), the maximum shear stress criterion (τ_{max}) and the maximum distortion energy criterion.

With these criteria, bearing in mind that radial stress σ_r and hoop stress σ_t are principal stresses, the equivalent or ideal stress σ_e is given by:

- σ_{max} criterion (Coulomb or Rankine criterion):

$$\sigma_e = max(|\sigma_t|;|\sigma_r|;|\sigma_z|) \ . \tag{9.1}$$

- ε_{max} criterion (Saint Venant criterion):

$$\sigma_e = max[|\sigma_t - \nu \cdot (\sigma_r + \sigma_z)|\,;|\sigma_r - \nu \cdot (\sigma_t + \sigma_z)|\,;|\sigma_z - \nu \cdot (\sigma_r + \sigma_z)|] \ . \tag{9.2}$$

V. Vullo and F. Vivio, *Rotors: Stress Analysis and Design*,
Mechanical Engineering Series, DOI 10.1007/978-88-470-2562-2_9,

- τ_{max} criterion (Tresca or Guest criterion):

$$\sigma_e = max(|\sigma_t - \sigma_r|;|\sigma_t - \sigma_z|;|\sigma_r - \sigma_z|). \tag{9.3}$$

- Maximum distortion energy criterion (Maxwell or Von Mises criterion):

$$\sigma_e^2 = \sigma_t^2 + \sigma_r^2 + \sigma_z^2 - \sigma_t \cdot \sigma_r - \sigma_r \cdot \sigma_z - \sigma_z \cdot \sigma_t. \tag{9.4}$$

To understand which failure criterion best interprets the experimental results, a few words are in order concerning the latter. Most available experimental results involve biaxial stress states. To compare data calculated with theoretical models and experimental data, it is necessary to consider plane (σ_r, σ_t). For the sake of convenience, it is also advisable to make stresses dimensionless by relating them to the equivalent stress σ_e, so that plane (σ_r, σ_t) becomes $(\sigma_r/\sigma_e, \sigma_t/\sigma_e)$.

The formulation of the maximum distortion energy criterion (the Von Mises criterion) in plane (σ_r, σ_t) translates into the equation of an ellipse, with semi-major and semi-minor diameters equal to $\sigma_e/\sqrt{2}$ and $\sigma_e\sqrt{2/3}$ respectively, positioned so that they bisect dihedra (σ_r, σ_t) and $(\sigma_r, -\sigma_t)$. This ellipse is represented in Fig. 9.1 on coordinates $(\sigma_r/\sigma_e, \sigma_t/\sigma_e)$.

As can be seen from the curve in Fig. 2.4, stress σ_t in an annular disk subjected only to negative internal pressure $\sigma_{ri} = -p_i$ is always tensile, while stress σ_r is always compressive, except at the outer radius where it is zero. At any radius, the values assumed by hoop stress are always greater than the absolute value of radial stress, or in other words the ratio $\sigma_t/|\sigma_r|$ is above unity at all times. Consequently, the arc of ellipse of interest to us here is that between the line bisecting dihedron $(-\sigma_r/\sigma_e, \sigma_t/\sigma_e)$ and the axis of stresses σ_t/σ_e i.e., the arc $\widehat{BC}$ whose correspondent in the fourth quadrant is arc $\widehat{B'C'}$.

As the curve in Fig. 2.2 shows, both stresses σ_r and σ_t in a radial thick-walled disk subjected only to external pressure $\sigma_{re} = -p_e$ are compressive (an exception is radial stress at the inner radius, which is zero). Here again, at any radius, the absolute value of hoop stress is always greater than the absolute value of radial stress, or in other words the ratio $|\sigma_t|/|\sigma_r|$ is above unity at all times. In this case, the arc of ellipse of interest to us here is that between the line bisecting dihedron $(-\sigma_r/\sigma_e, -\sigma_t/\sigma_e)$ and the negative part of the σ_t/σ_e axis, i.e., the arc $\widehat{A'B'}$, whose correspondent in the first quadrant is arc $\widehat{AB}$.

If the failure criterion used is that of maximum shear stress (the Tresca or Guest criterion), instead of having the Von Mises ellipse on coordinates (σ_r, σ_t), we will have the failure polygon (hexagon) as shown on coordinates $(\sigma_r/\sigma_e, \sigma_t/\sigma_e)$ in Fig. 9.1. With the same approach as used for the maximum-distortion-energy failure criterion, we can conclude that the parts of this failure polygon of interest in the rotors and disks design are respectively the straight-line $\overline{BF}$, which corresponds to straight-line $\overline{DF'}$, and straight-line $\overline{A'B'}$ corresponding to straight-line $\overline{AB}$.

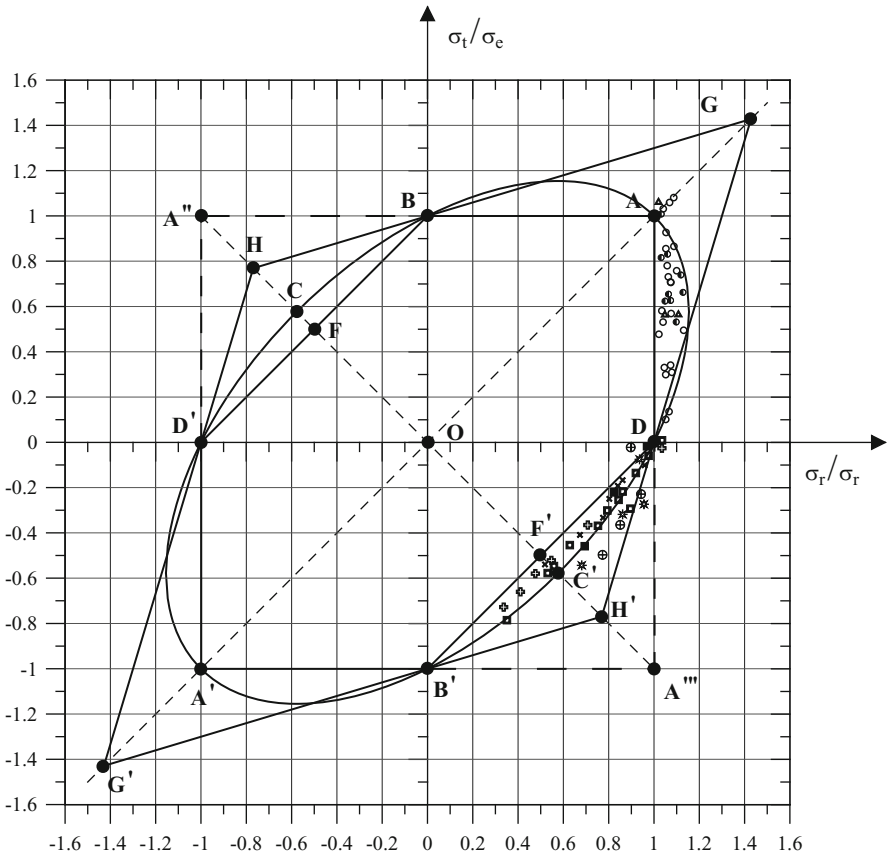

Fig. 9.1 Plane stress failure curves of maximum-distortion energy ellipse, maximum-shear-stress hexagon, maximum-normal-stress square and maximum-normal-strain rhombus on coordinates $(\sigma_r/\sigma_e, \sigma_t/\sigma_e)$

It should be noted that the maximum distortion energy failure criterion can be regarded as the generalization of the τ_{max} criterion, in that it also considers the influence exerted by the third principal stress on yielding. To be handled as a generalization of the τ_{max} criterion, it must be seen as a maximum octahedral shear stress criterion $\tau_{oct,max}$. As we know from continuum mechanics, the stresses acting in the eight octahedral planes, each of which is obtained by cutting across one of the corners of a principal element (a cubical element stressed by the three principal stresses $\sigma_1, \sigma_2, \sigma_3$), have interesting and significant properties. In fact, the same normal stress acts on each of the eight octahedral planes delimiting the octahedron thus obtained. This stress state, a hydrostatic stress state, tends to compress or enlarge the octahedron homothetically, without distorting it, with a consequent variation in volume but not in shape. The shear stresses acting on each of the eight octahedral planes are also equal, but they tend to distort the octahedron without changing its volume. Although the octahedral shear stress is less than the

maximum principal shear stress (in this connection, it should be borne in mind that in Mohr's plane $\tau = \tau(\sigma)$, the octahedral stresses are represented by the points outside the two smaller Mohr's circles and inside the principal Mohr's circle, or in other words lie in the area between these circles), it is a single value which depends on all three principal stresses $(\sigma_1, \sigma_2, \sigma_3)$.

The following relations express the octahedral normal stress and the octahedral shear stress as a function of the three principal stresses.

$$\sigma_{oct} = \frac{1}{3}(\sigma_1 + \sigma_2 + \sigma_3) \tag{9.5}$$

$$\tau_{oct} = \frac{1}{3}\left[(\sigma_1 - \sigma_2)^2 + (\sigma_2 - \sigma_3)^2 + (\sigma_3 - \sigma_1)^2\right]^{1/2}. \tag{9.6}$$

The octahedral-shear-stress can also be expressed as a function of the three principal-shear-stresses $\tau_{1,2}$, $\tau_{1,3}$, $\tau_{2,3}$ (i.e., the maximum values of the shear stresses correlated with the three Mohr's circles in Mohr's plane) as follows:

$$\tau_{oct} = \frac{2}{3}\left[\tau_{1,2}^2 + \tau_{1,3}^2 + \tau_{2,3}^2\right]^{1/2}. \tag{9.7}$$

According to the maximum octahedral shear stress criterion, the strength limit condition will be reached when

$$(\sigma_1 - \sigma_2)^2 + (\sigma_2 - \sigma_3)^2 + (\sigma_3 - \sigma_1)^2 = 2\sigma_e^2. \tag{9.8}$$

This relation, where $\sigma_1 = \sigma_t, \sigma_2 = \sigma_z$ and $\sigma_3 = \sigma_r$, is linked to relation (9.4), or in other words to the maximum distortion energy failure criterion.

Figure 9.1 also shows the geometric loci which represent the other two failure criteria considered, viz., the σ_{max} and the ε_{max} criteria, on coordinates $(\sigma_r/\sigma_e, \sigma_t/\sigma_e)$. In this plane, the maximum-normal-stress yield criterion translates into the failure square obtained by extending, pairwise, sides $\overline{AB}$ and $\overline{A'B'}$ and sides $\overline{AD}$ and $\overline{A'D'}$ until they meet. Lastly, the maximum normal strain failure criterion translates into the failure rhombus whose major and minor diagonals are superimposed on the semi-major and semi-minor diameters of the failure ellipse, and whose four sides pass through points B, D, B' and D' and converge pairwise on the points lying on the major diagonal having coordinates $[1/(1-\nu), 1/(1-\nu)]$ and $[-1/(1-\nu), -1/(1-\nu)]$ respectively.

Mohr's failure criterion assumes that the strength limit conditions occurs when the stress state is represented by the points in Mohr's plane $\tau = \tau(\sigma)$ that lie on the envelope of the infinite Mohr's circles for stress states at the limit of failure onset. In Mohr's plane, this envelope is represented by two nonlinear curves that are symmetrical with respect to the axis of the abscissas (σ axis) and converge on a point of the latter with a positive abscissa, where the material breaks as a result of cohesive failure (Fig. 9.2). These curves become two straight lines (simplified Mohr's criterion), again symmetrical with respect to the σ axis and converging on a point

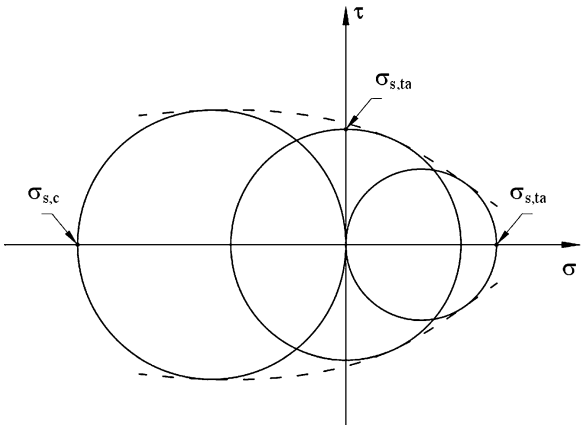

Fig. 9.2 Mohr's criterion for biaxial stress represented on Mohr plane $\tau = \tau\,(\sigma)$

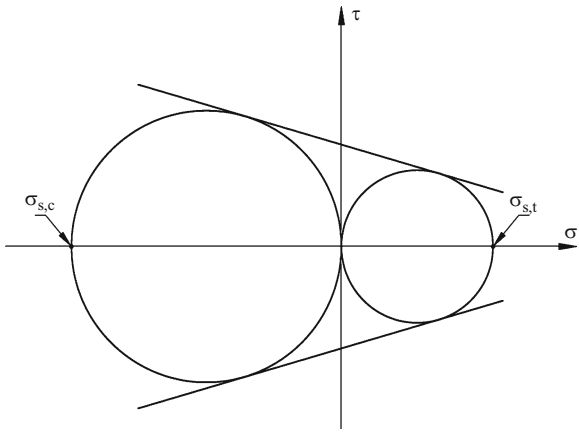

Fig. 9.3 Simplified Mohr's criterion for biaxial stress represented on Mohr plane $\tau = \tau\,(\sigma)$

of the latter having coordinates ($\sigma > 0$, $\tau = 0$), in the case where the experimental data used are provided by two uniaxial tests, the first uniaxial tension test and the second uniaxial compression test (Fig. 9.3). From this standpoint, Mohr's criterion can be considered as a modification of the τ_{max} criterion.

In plane (σ_1, σ_2), Mohr's criterion for the biaxial stress state results in two nonlinear curves that are symmetrical with respect to the diagonal bisecting the dihedra of the first and third quadrants. The points where these two curves (Fig. 9.4) intersect the coordinate axes and the shear diagonal (the straight-line bisecting the dihedra of the second and fourth quadrants) can be readily identified by means of uniaxial tension and compression data and pure shear data. The upper curve will thus intersect the axis of the abscissa at the point whose coordinates are $(-\sigma_{f,c}, 0)$, the axis of the ordinate at the point whose coordinates are $(0, \sigma_{f,t})$ and the shear diagonal at the point whose coordinates are $(\sigma_{f,ta}, \sigma_{f,ta})$, where $\sigma_{f,t}$, $\sigma_{f,c}$ and $\sigma_{f,ta}$ are the failure limit stresses in uniaxial tension test, compression test and pure shear test, respectively. For the lower curve, the points of intersection with the three straight lines can be identified through the symmetry indicated above.

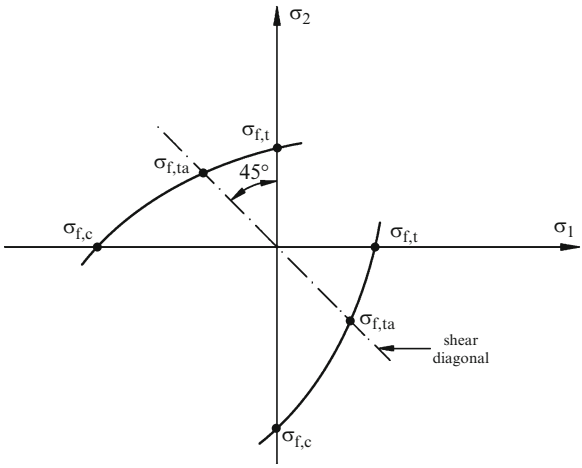

Fig. 9.4 Mohr's criterion for biaxial stress represented on coordinates (σ_1, σ_2)

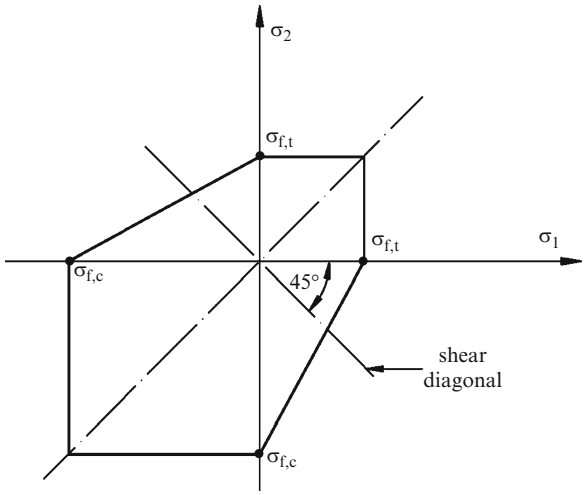

Fig. 9.5 Failure strength closed irregular polygon of the simplified Mohr's criterion for biaxial stress represented on coordinates (σ_1, σ_2)

Just as the two straight lines in Fig. 9.3, which are symmetrical with respect to the axis of the abscissa, are an approximate representation of the two curves in Fig. 9.2 for Mohr's criterion in Mohr's plane, in plane (σ_1, σ_2), the two curves in Fig. 9.4 can be represented by a closed irregular hexagon, whose sides differ in the first and third quadrants (Fig. 9.5). This is the strength limit hexagon for Mohr's simplified criterion. From this standpoint as well, Mohr's criterion can be considered as a modification of the τ_{max} criterion.

In other words, the $\tau = \tau(\sigma)$ and $\sigma_2 = \sigma_2(\sigma_1)$ curves for Mohr's criterion can be obtained starting from the corresponding curves for the τ_{max} criterion, considering and including the effect of internal friction. For this reason Mohr's criterion is also called the internal-friction-criterion. Proposed in 1897 by Reyto, this criterion assumes that sliding along the slip planes is inhibited by the friction forces associated with the compressive forces acting orthogonally to said planes.

In plane (σ_1, σ_2), Mohr's criterion in its generalized formulation, i.e., that using comprehensive experimental data, leads to a closed curve like the failure strength ellipse, but asymmetrical with respect to the shear diagonal. It is thus an ovoid, larger in the third quadrant and smaller in the first quadrant, but still symmetrical with respect to the straight-line bisecting the first and third quadrants. Mohr's criterion is thus more general than the maximum distortion energy criterion, in that it can account for and simulate the material's differing behaviour in compression and tension.

9.2 General Considerations on the Use of Failure Criteria

The main failure criteria applied in the design sector of interest to us here were discussed in the preceding section. To choose the best criterion for use, however, they must be re-examined in the light of the experimental results obtained by the various researchers who have addressed this topic. To achieve the desired biaxial stress state, many of these researchers have used thin-walled steel, copper and aluminium tubes subjected simultaneously to internal pressure and to axial and torsional loading, or tubes under combined tensile and torsional loading. Most of the results obtained, all from tests at ambient temperature, consist of points representing stress states in the first and fourth quadrants, and which are denser around the maximum-distortion-energy failure ellipse or, at most, fall in the zones between the straight lines of the strength limit hexagon and the corresponding curve segments of the strength limit ellipse. The location of these experimental points, which are shown in Fig. 9.1, demonstrates unequivocally that the failure criterion that best interprets experimental findings is that of maximum-distortion-energy.

For certain load combinations, several of the four main failure criteria (σ_{max}, τ_{max}, ε_{max} and maximum-distortion-energy) provide the same results, and are equally advantageous. In other cases, the results of the theoretical models differ, and the problem thus arises of selecting the criterion that best interprets the actual risk of failure in the material. Generally speaking, it must be recognized that there is no single criterion: we can only identify the criterion that is best for a particular purpose. The same criterion applied in different situations may result in errors. For example, repeated experimental tests have demonstrated that yield strength in torsional is about 12–15 % higher than the shear strength determined through tensile testing. This discrepancy, though it can be explained theoretically, would not arise if the τ_{max} criterion were correct. The maximum-distortion-energy criterion does not suffer from this limitation, and its accuracy is borne out both by theoretical considerations and experimental findings, making it the optimal choice among the different failure criteria at least for ductile materials.

A number of tests carried out on specimens consisting of cast iron or other brittle materials have led to the conclusion that the σ_{max} failure criterion is better for brittle materials than the other criteria. However, data from more accurate tests conducted in recent years have clearly demonstrated that the behaviour of brittle materials can

be effectively interpreted by the maximum distortion energy criterion, providing that account is made for the effects of stress concentrations resulting from the inclusions that often cause a structural component to lose ductility.

Lastly, the ε_{max} failure criterion, widely used in the nineteenth century and the first half of the twentieth, particularly in the design of artillery and of porcelain and reinforced concrete components, has been largely abandoned today. Here, it is not used.

From the general design standpoint, in any case, the σ_{max} failure criterion can also be used with success, providing that the stress state is represented by points falling in the first and third quadrants of Fig. 9.1. In the first quadrant, both stresses are positive and the σ_{max} and τ_{max} criteria lead to the same results. When the principal stresses are all equal, the three σ_{max}, τ_{max} and maximum distortion energy criteria lead to the same results. If the stress state is represented by points falling in the second and third quadrants, it is obvious that only the τ_{max} and maximum distortion energy criteria can be used.

In mechanical design, the material's failure criterion is selected and used on the basis of more general considerations. In these pages, we are dealing with operating conditions that do not involve excessive elastic displacements, instability, creep, impact and fatigue, all of which call for further and more specific considerations. Notch effects and stress concentrations are considered as localised effects in the areas affected by the geometrical irregularities. The fatigue aspects are not considered. Attention focuses here on static and quasi-static.

Where a preliminary review of actual design conditions indicates that component failure may take place during service with modes that differ from those found for standard specimens, it is obvious that the failure criteria discussed above cannot be applied. To give an example, if it is suspected that brittle fracture could occur in a component consisting of normally ductile steel, none of these criteria is capable of linking this condition to the data obtained from standard tensile tests. In such a situation, it will be necessary to use more advanced theoretical considerations and experimental data from specific tests (impact tests, for instance) carried out under conditions that approximate those encountered during actual service to the greatest possible extent.

We will now focus attention on cases where the material failure criteria can be correctly applied, starting from their use in predicting ductile yielding. Here, the criterion that interprets experimental results most accurately is that of the maximum distortion energy. It is thus recommended that it be used, though with some reservations. For the biaxial stress state, when good experimental data are available that go beyond those from simple tensile tests, Mohr's criterion is to be preferred. In this connection, however, a possible weakness of Mohr's criterion should be noted: as it is difficult to obtain highly accurate compression and tension data (i.e., giving as general an idea as possible regarding the stress state in experimental conditions), the errors may greater than those associated with the maximum distortion energy criterion.

For triaxial stress states, the amount of data available is relatively modest. The maximum distortion energy criterion can nevertheless be applied with good results, but there is also no lack of grounds for recommending that the more conservative

internal-friction-criterion be used. For both biaxial and triaxial stress states, it is still fairly common to use the simple and slightly conservative τ_{max} criterion together with data from standard tensile tests. Many regulations and calculation standards are based on this criterion.

The predictive criteria for ductile fracture coincide in general with the predictive criteria for yielding. However, the experimental data available in this connection are not only more limited numerically, but also show greater scatter. For these reasons, it is sometimes recommended that the internal-friction-criterion be used instead of the maximum-distortion-energy criterion.

To predict the failure strength of materials that can be affected by brittle fractures in simple tension and compression, it is once again necessary to have reliable experimental data. For biaxial stress states, Mohr's criterion can be used. The internal-friction-criterion can be employed if uniaxial tension and compression data are available, and is reasonably accurate. It is often recommended for this reason, but the results obtained are in general conservative. The σ_{max} criterion is occasionally used, but it often leads to results that, for biaxial tension-compression stress states, can be affected by significant errors, as they are heavily skewed towards the non-conservative side. Experimental results obtained by a number of researchers on the basis of tests conducted on grey cast iron are clearly included between the theoretical curves for the σ_{max} criterion and the internal-friction-criterion, which are thus in agreement when a biaxial stress state is considered.

9.3 Effects of Stress Concentrations

It was mentioned earlier that rotors generally have irregularities in form, most frequently because of holes provided for purposes such as retaining the rotor to the machine, attaching parts to the disk or channeling cooling fluids. If the hole is small by comparison with the size of the disk, or if the distance between two successive holes is much larger than their radius, the effect of the holes can be considered as a local disturbance of the stress field calculated assuming axisymmetry.

For an isolated hole of small diameter $2{\cdot}r_i$ centred along the axis of a thin-walled rectangular plate, having short sides of dimension $2{\cdot}r_e >> 2{\cdot}r_i$ and stressed on the mid-plane of the short sides by a uniform surface force distribution σ (Fig. 9.6), an elegant theoretical solution presented by Kirsch [38], which has been confirmed experimentally through strain gauge and photoelastic analyses, can be used to determine the stress state on the hole's periphery through the superposition of two stress states (Fig. 9.7) for the plate with central hole whose outer radius $2{\cdot}r_e$ is indicated by the dashed line in Fig. 9.6.

The first stress state sees the plate as subjected in its mid-plane and at its outer radius to a uniform radial stress distribution $\sigma/2$, while the second sees the same plate as simultaneously subjected, again in its mid-plane and at its outer radius, to a radial stress distribution $(\sigma/2){\cdot}cos\ 2\vartheta$ and a shear stress distribution $-(\sigma/2){\cdot}sin\ 2\vartheta$

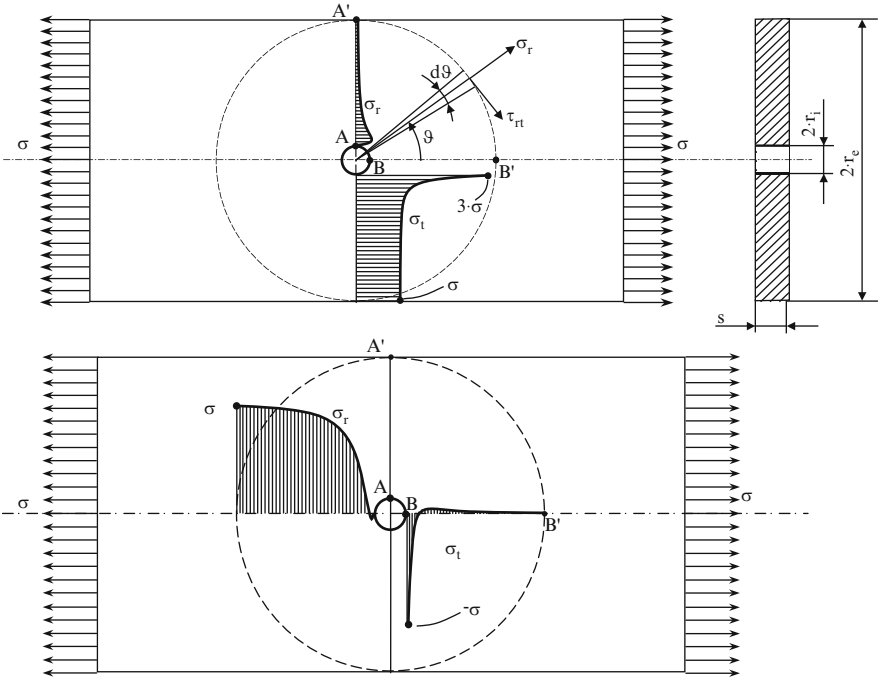

Fig. 9.6 Thin rectangular sheet with central hole whose radius r_i is small compared to r_e, stressed on the short sides and in the mid-plane by a surface force distribution σ

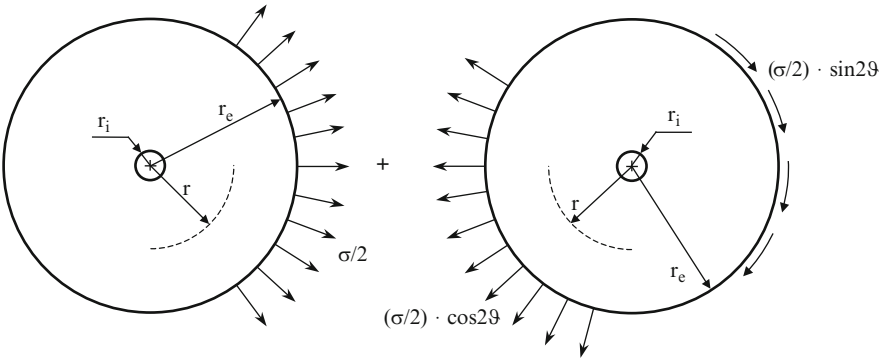

Fig. 9.7 Superposition of two stress states for analysing the stress state of the circular plate take from the rectangular plate shown in Fig. 9.6

(the minus sign indicates that, as illustrated in Fig. 9.6, the shear stress acts in the opposite direction to the increasing angular coordinates ϑ).

The results obtained by Kirsch through the modelling procedure described above enable us to express the stress state at the generic radius r and at the generic angular coordinate ϑ with the following relations:

$$\begin{cases} \sigma_r = \dfrac{\sigma}{2} \cdot \left(1 - \dfrac{r_i^2}{r^2}\right) + \dfrac{\sigma}{2} \cdot \left(1 + \dfrac{3 \cdot r_i^4}{r^4} - \dfrac{4 \cdot r_i^2}{r^2}\right) \cdot cos\, 2\vartheta \\ \sigma_t = \dfrac{\sigma}{2} \cdot \left(1 + \dfrac{r_i^2}{r^2}\right) - \dfrac{\sigma}{2} \cdot \left(1 + \dfrac{3 \cdot r_i^4}{r^4}\right) \cdot cos\, 2\vartheta \\ \tau_{rt} = -\dfrac{\sigma}{2} \cdot \left(1 - \dfrac{3 \cdot r_i^4}{r^4} + \dfrac{2 \cdot r_i^2}{r^2}\right) \cdot sin\, 2\vartheta. \end{cases} \tag{9.9}$$

These relations derive from the more general relations, neglecting the ratio r_i^2/r_e^2 and, even more importantly, the ratio r_i^4/r_e^4 in the latter. It can thus be concluded that the stress state in points A, A', B and B' in Fig. 9.6 is characterized by the following values:

$$\begin{array}{lllll} A(r = r_i; \vartheta = \pi/2): & \sigma_r = 0; & \sigma_t = 3 \cdot \sigma; & \tau_{rt} = 0 \\ A'(r = r_e; \vartheta = \pi/2): & \sigma_r = 0; & \sigma_t = \sigma; & \tau_{rt} = 0 \\ B(r = r_i; \vartheta = 0): & \sigma_r = 0; & \sigma_t = -\sigma; & \tau_{rt} = 0 \\ B'(r = r_e; \vartheta = 0): & \sigma_r = \sigma; & \sigma_t = 0; & \tau_{rt} = 0. \end{array}$$

These results show that along the periphery of the hole, at the ends of the diameter perpendicular to the direction of loading, the only non-zero stress is the hoop stress, which is $3{\cdot}\sigma$ at A and σ at A'. At the ends of the diameter parallel to the direction of loading, stresses at the hole periphery, i.e., at B, are $\sigma_t = -\sigma$ and $\sigma_r = \sigma$ at B', while all other stresses are zero. Figure 9.6 shows hoop stress σ_t and radial stress σ_r versus radius, both in direction A-A' perpendicular to the loading axis, and in direction B-B' parallel to the direction of stresses σ. The curve for σ_t shows that we have $\sigma_t = 3{\cdot}\sigma$ at A and $\sigma_t = -\sigma$ in B. The stress concentration resulting from the hole thus leads to a threefold increase in the value of applied stress σ localized at A.

For a plate subjected to uniaxial stress along the direction indicated in Fig. 9.6, we have the result summarized in Fig. 9.8a. If the same plate is stressed at its mid-plane, along two mutually orthogonal directions (A-A' and B-B' in Fig. 9.6) by uniformly distributed surface forces σ_1 and σ_2, we can apply the principle of superposition to obtain the result shown in Fig. 9.8b.

However, the problem of interest to us here is that of a rotating disk featuring a small-diameter eccentric hole with axis parallel to that of the rotor and located at a distance r from it. Once the stresses σ_r and σ_t that we would have at the position occupied by the centre of the hole if the latter did not exist have been calculated, it is obvious that a rectangular plate element such as that represented in Fig. 9.6 can be identified, with direction A-A' along the radial passing through the centre of the hole. In this case, bearing Fig. 9.8b in mind, we have $\sigma_1 = \sigma_t$ and $\sigma_2 = \sigma_r$.

Applying Kirsch's theory to this specific case thus enables us to quantify the maximum stresses at the periphery of the hole as follows:

$$\begin{aligned} \sigma_{t,max} &= 3 \cdot \sigma_t - \sigma_r \\ \sigma_{r,max} &= 3 \cdot \sigma_r - \sigma_t, \end{aligned} \tag{9.10}$$

where, as we have said, σ_t and σ_r are the stresses that would occur at the position occupied by the centre of the hole if the hole did not exist. Stresses (9.10) act

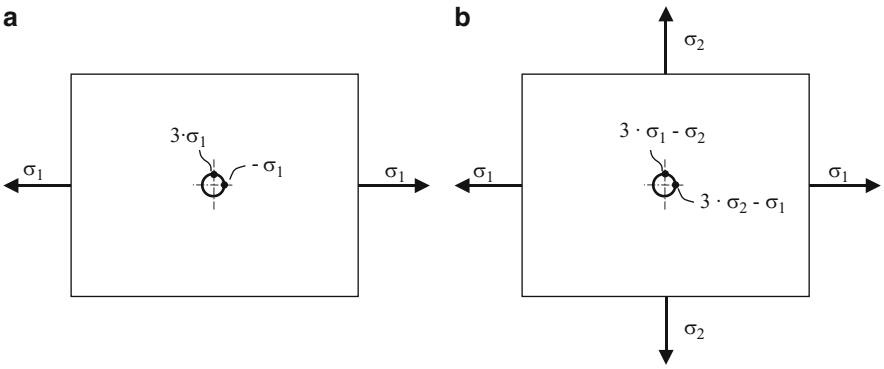

Fig. 9.8 Values of hoop stress σ_t at points A and B indicated in Fig. 9.6: (**a**) uniaxial stress; (**b**) biaxial stress

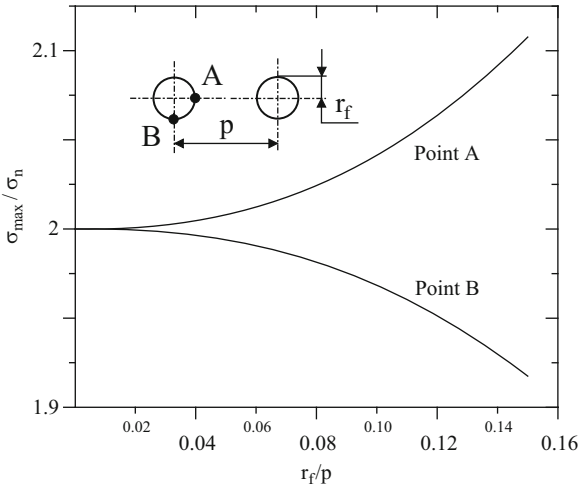

Fig. 9.9 Ratio σ_{max}/σ_n at edge of holes versus ratio r_f/p

tangentially to the edge of the hole and are found at the ends of the diameter whose extension passes through the centre of the disk and at the ends of the diameter perpendicular to the first.

The small-diameter central hole can be regarded as the limiting case of an eccentric hole as the distance of its axis from the disk axis tends to zero. In this case, σ_r and σ_t tend to be equal and the value at the edge of the hole tends to a value which is twice that which it would assume if there were no hole.

It also follows from relations (9.10) that making a hole in a uniform strength disk ($\sigma_t = \sigma_r = \sigma$) doubles the value of the stress, regardless of point where the hole is located.

If there is an array of holes, it should be borne in mind that the increase in stress will be greater than that which would occur with a single hole. By way of example, Fig. 9.9 shows the ratio (σ_{max}/σ_n) of maximum stress at the edge of the holes to

nominal stress σ, versus ratio r_f/p of hole radius to spacing for a uniform strength disk. Consequently, it is good design practice to avoid holes in favour of other methods of securing highly stressed disks to the shaft.

To evaluate stress concentrations in fillets, notches and any other irregularities in form, it is necessary to use numerical discretization techniques such as the finite element method.